JOM Journal of Optical Microsystems

RESEARCH PAPER

Fourier scatterometry for compensation of tilt and curvature deviations of two-photon polymerization three-dimensional printers

Elias Ellingen,* Markus Rohde, Bastian Stahl, and Robert Lange
Bonn-Rhein-Sieg University of Applied Sciences, Institute of Safety and Security Research (ISF), Sankt Augustin, Germany

ABSTRACT. A Fourier scatterometry setup is evaluated to recover the key parameters of optical phase gratings. Based on these parameters, systematic errors in the printing process of two-photon polymerization (TPP) gray-scale lithography three-dimensional printers can be compensated, namely tilt and curvature deviations. The proposed setup is significantly cheaper than a confocal microscope, which is usually used to determine calibration parameters for compensation of the TPP printing process. The grating parameters recovered this way are compared to those obtained with a confocal microscope. A clear correlation between confocal and scatterometric measurements is first shown for structures containing either tilt or curvature. The correlation is also shown for structures containing a mixture of tilt and curvature errors (squared Pearson coefficient $r^2 = 0.92$). This compensation method is demonstrated on a TPP printer: a diffractive optical element printed with correction parameters obtained from Fourier scatterometry shows a significant reduction in noise as compared to the uncompensated system. This verifies the successful reduction of tilt and curvature errors. Further improvements of the method are proposed, which may enable the measurements to become more precise than confocal measurements in the future, since scatterometry is not affected by the diffraction limit.

© The Authors. Published by SPIE under a Creative Commons Attribution 4.0 International License. Distribution or reproduction of this work in whole or in part requires full attribution of the original publication, including its DOI. [DOI: 10.1117/1.JOM.3.4.043501]

Keywords: grating reconstruction; two-photon polymerization; transmission phase gratings; Fourier scatterometry

Paper 23020G received Aug. 9, 2023; revised Oct. 13, 2023; accepted Oct. 20, 2023; published Nov. 6, 2023.

1 Introduction

Two-photon polymerization (TPP) is an additive manufacturing technique for the fabrication of micro-scale structures for a multitude of applications.[1] An important one is the fabrication of diffractive optical elements (DOEs). In TPP, a laser beam is focused into a resin, usually through a microscope objective. The resin is only polymerized near the focus spot. The focus spot can be moved within the field of view of the objective by a galvano mirror set. The size of the polymerized area can be changed by adjusting laser power. To allow the printing of structures larger than the objective field of view, the substrate can additionally be moved by a piezoelectric stage. This way, larger structures can be stitched together.[2]

However, undesired tilt of the substrate holder or aberrations of the objective can affect every printing field and manifest as periodic errors in these stitched structures. This effect is shown in Figs. 1(a) and 1(d). The figure further shows the undesired grating, created by tilt errors and

*Address all correspondence to Elias Ellingen, elias.ellingen@smail.emt.h-brs.de

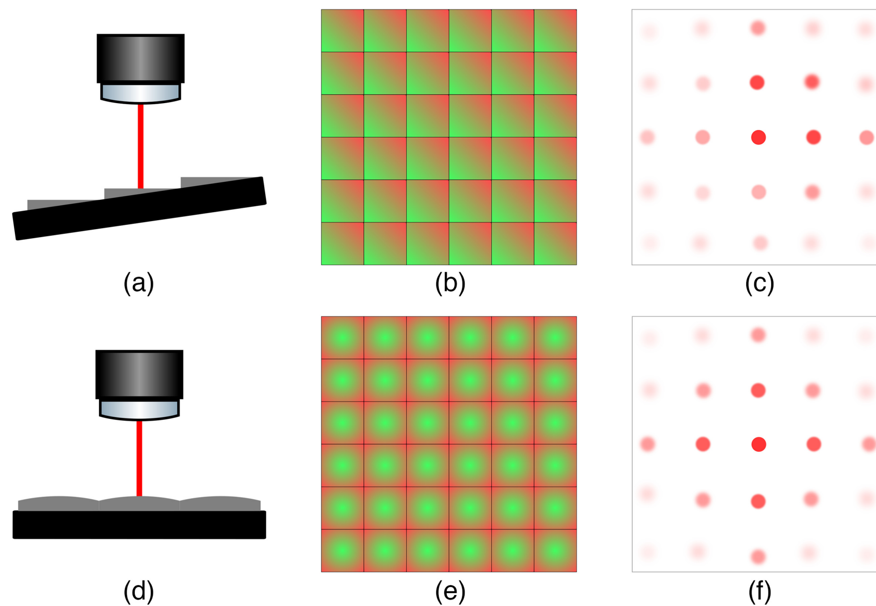

Fig. 1 Periodic errors of the TPP printing process caused by stitching of the printing fields. (a)–(c) The cause and effect of tilt errors and (d)–(f) the cause and effect of curvature errors. (a), (d) The root cause of the errors: a tilt of the substrate holder leads to tilted stitching fields. The curved focus plane of the objective leads to a curved surface on each block since TPP only occurs in the focus spot. (b), (e) The resulting phase grating structures (color representing the height). (c), (f) The theoretical far-field diffraction patterns for coherent illumination.

curvature errors, as shown in Figs. 1(b) and 1(e), respectively. Finally, the far-field diffraction pattern of tilt gratings and curvature gratings is shown in Figs. 1(c) and 1(f), respectively. These are calculated as the two-dimensional Fourier transform of the complex grating transmission function. In practice, these errors can be compensated by measuring tilt and curvature errors and subtracting them from subsequent design files. The compensation data are obtained by printing a structure designed to be flat. It will show the periodic errors as discussed, which can then be measured. To perform this measurement, a confocal microscope is usually required. Other surface metrology techniques, such as white light interferometry or atomic force microscopy (AFM), can also be used to find the tilt and curvature errors. However, white light interferometry may lead to improper height measurements near steps, which frequently occurs in our structures.[3] AFM is limited to measurement of small structures.[4] All these measurement devices are fairly expensive.

In this work, we investigate whether a scatterometric setup can be used instead of a confocal microscope, possibly reducing cost and improving precision. Figure 2 illustrates the general idea: a grating (a) produces a diffraction pattern (c) from which a reconstructed grating (b) is derived.

Scatterometry is already widely used in critical dimension monitoring for semiconductor manufacturing. It has also previously been used to characterize structures produced by TPP.[5] These previous approaches are usually based on an optical setup, including beam splitters, digital cameras, and high NA microscope objectives, used to measure the scattered light intensity distribution. In combination with a sophisticated reconstruction software, the grating parameters can be reconstructed with nanometer accuracy.[6]

We present a simpler optical setup, only consisting of a coherent light source, an aperture stop, and an integrating sphere, which is moved along a linear translation stage perpendicular to the optical axis. This way, the intensity of multiple diffraction orders can be measured. We evaluate whether this low cost setup is suitable to perform tilt and curvature compensation on a TPP printer (Nanoscribe QuantumX) by testing the correlation between reconstructed grating parameters and confocal measurement of the grating parameters. From this data, we also estimate the accuracy at which we can determine grating parameters. We then show the effect of this compensation on images produced by diffractive optical elements. Results obtained with the compensation are compared to the uncompensated system. In this context, we also discuss the qualitative effects of tilt and curvature errors on structures produced with a TPP printer.

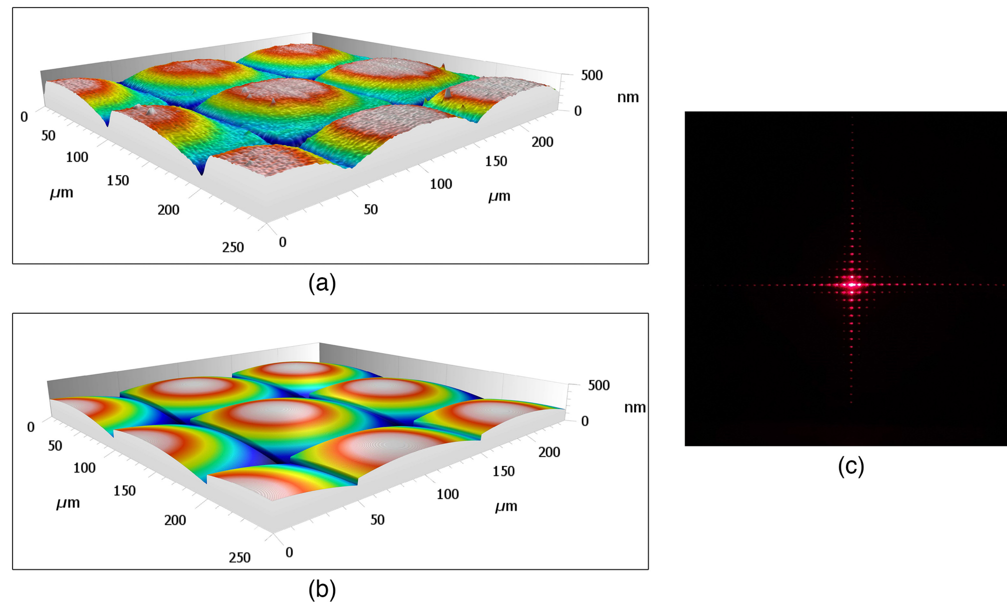

Fig. 2 Application of scatterometry for the reconstruction of gratings. (a) The result of confocal measurement of a test grating, (b) the reconstructed phase grating and (c) the measured diffraction pattern. The parameters of this grating are determined from (c) with our scatterometry approach.

2 Methods

2.1 Scatterometry

Today, scatterometry is widely used in critical dimension monitoring for semiconductor manufacturing. A good overview is given in Ref. 7: light scattered by a grating is analyzed under variation of parameters, such as the illumination wavelength or angle of incidence. The grating parameters are then reconstructed from the measured variation in the intensity data of the diffraction pattern. This reconstruction is usually achieved either by an optimization approach or by a library search method. Both attempt to find the set of parameters most likely causing the measured intensity distribution. Usually, a so called forward-model is used to simulate the intensity data for a given set of grating parameters. The most common model is "rigorous coupled wave analysis" (RCWA) but historically Fraunhofer diffraction has also been used.

In this work, we present a less complex solution since the accuracy requirements for this proof of concept are lower than in later applications. The optimization approach is applied with a simplified forward model, based on the Rayleigh–Sommerfeld convolution.[8] While RCWA is a rigorous vector wave theory, Rayleigh–Sommerfeld convolution is based on scalar wave theory. It is assumed that this less rigorous approach approximates the far-field intensity distribution sufficiently, considering that the proposed setup does not measure polarization. This approach is simple to implement since the Rayleigh–Sommerfeld convolution is available through the Python package "diffractio."[9] Multiple nonlinear optimization algorithms are also available through Python packages, such as scipy.[10]

2.2 Forward Model

The forward model describes a way to calculate intensity data for a given set of grating parameters. First, a function to model the effect of the grating on the incident field is required. Assuming the parasitic grating can be described exclusively by tilt and curvature errors, the surface of one period of this grating can be modeled as a second-degree polynomial

$$h(x, y) = a_x \cdot x + b_x \cdot x^2 + a_y \cdot y + b_y \cdot y^2 \quad x, y \in \left[-\frac{d}{2}, \frac{d}{2}\right], \tag{1}$$

where a_x and a_y describe the tilt errors; b_x and b_y describe the curvature errors along the x and y-axis, respectively; and d is the period of the grating. Without loss of generality only

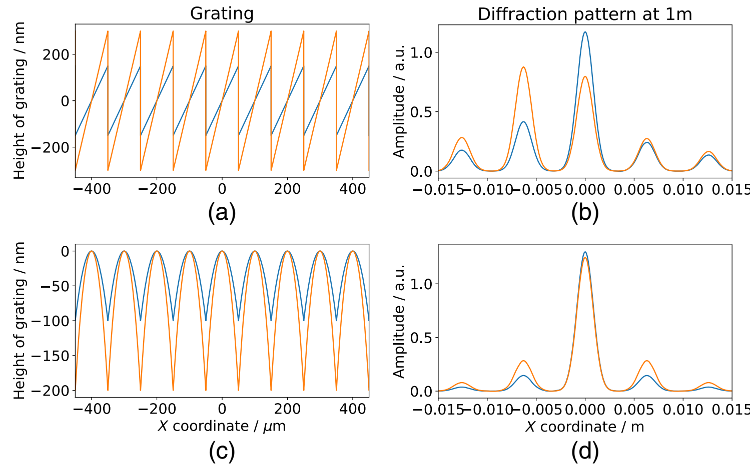

Fig. 3 Tilted and curved gratings and their diffraction patterns: For two tilted gratings (a) the far-field diffraction patterns (b) are simulated. Similarly (c) shows two curved gratings and (d) shows their far-field diffraction image. The simulation uses a wavelength of 630 nm.

the x component will be considered in the following sections, all steps apply to the y component the same way. A periodic continuation of this function is given as

$$h(x) = a_x \cdot (x - m \cdot d) + b_x \cdot (x - m \cdot d)^2 \quad x \in \left[-\frac{d}{2}, \frac{d}{2}\right], m \in \mathbb{N}. \tag{2}$$

Assuming the grating has a constant refractive index n_1 and is placed inside a medium with constant refractive index n_0, the phase shift induced by the grating is

$$\phi(x) = h(x)\frac{2\pi \cdot (n_0 - n_1)}{\lambda}. \tag{3}$$

As described in Ref. 11, the scalar field $U(x)$ occurring directly after this grating is then

$$U(x) = T(x) \cdot U_{\mathrm{in}}(x) \cdot e^{-i \cdot \phi(x)}, \tag{4}$$

where $U_{\mathrm{in}}(x)$ describes the incident field and $T(x)$ describes the transmission of the grating at each point. We assume that the grating transmits all the light within the aperture, resulting in

$$T(x) = \begin{cases} 1 & \text{if } x \in [-r, r] \\ 0 & \text{if } x \notin [-r, r], \end{cases} \tag{5}$$

where r is the radius of the aperture. To approximate the incident field, a constant phase is assumed, along with the typical laser intensity distribution given in the laser data sheet. This field $U(x)$ can then be passed to the Rayleigh–Sommerfeld algorithm implemented in Ref. 9 to obtain the field $U_{\mathrm{out}}(x)$ at a certain distance. In our setup, the intensity of this field is sampled with an integrating sphere around multiple maxima. To take this into account, all simulated intensity data points that would fall within the opening of the integrating sphere are integrated. This way a set of simulated intensities $I_{k,\mathrm{sim}}(a, b)$ at the k'th maxima is obtained. Figure 3 shows tilted and curved structures and the simulated amplitudes in the farfield, assuming they are illuminated with a 635 nm coherent light source.

The sum of these steps together is the forward model: for a certain combination of grating parameters $[a, b]$, the field $U(x)$ behind the grating is calculated, the far-field intensity distribution is calculated via Rayleigh–Sommerfeld diffraction, and this intensity distribution is sampled around the maxima, resulting in simulated intensity values $I_{k,\mathrm{sim}}(a, b)$, for the k_{th} maximum.

2.3 Inverse Problem

Given n intensity data measurements, the reconstruction of grating parameters can be formulated as a least-squares minimization problem

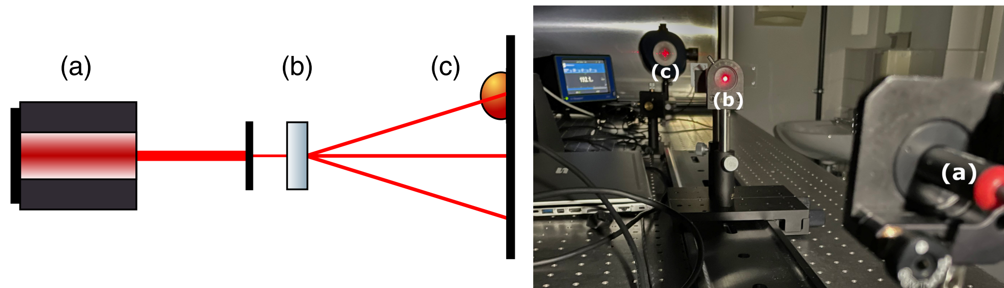

Fig. 4 Measurement setup: the laser (a) emits coherent light, which passes through an aperture stop and the grating under test (b). The intensity of the diffraction orders is measured using a movable integrating sphere (c).

$$a, b = \arg\min_{a,b}\left[\sum_{k=1}^{n}(I_{k,\mathrm{sim}}(a,b) - I_{k,\mathrm{meas}})^2\right], \tag{6}$$

where $I_{k,\mathrm{sim}}(a,b)$ is the set of simulated intensity values, whereas $I_{k,\mathrm{meas}}$ are the measured intensity values. A solution for this problem is implemented in the Python package "scipy." Given a function that implements the forward model, the measured data points and a set of starting values for a and b, the parameters resulting in a local minimum are returned. For these local optimization routines, the choice of starting values is highly influential.[7] We use $a = 3 \times 10^{-3}$ and $b = 100\ \mathrm{m}^{-1}$ for all tested structures. These starting values are typical parameters for tilt and curvature errors of the used print-set. Our test structures are chosen around these parameters. The estimated uncertainty of the parameters is also returned by the minimization routine.

2.4 Measurement Setup

The measurement setup consists of three parts, as shown in Fig. 4: a coherent light source (a), the grating under test along with an aperture stop (b), and a movable detector (c).

The light source, a 635 nm laser, with optical power of 1 mW (Thorlabs PL204), is placed at a distance of one meter from the grating. An aperture stop of 1 mm diameter is placed in front of the grating, to ensure that all light is transmitted solely through the grating itself, rather than bypassing it at the edges. At a propagation distance of one meter, a linear translation stage carrying an adjustable integrating sphere is placed perpendicular to the optical axis. The opening of the integrating sphere is small enough to measure single diffraction maxima.

During measurement, the integrating sphere is manually moved toward different diffraction orders. To find the maximum for each diffraction order, the position is varied until the measured intensity is maximal. The intensity at each diffraction order is then used to reconstruct the grating parameters.

The duration of the measurement of a diffraction pattern using the Fourier scatterometry setup is about 5 min, compared to about 30 s with a confocal microscope. An alternative to reduce the measurement time of this setup could be to use a high dynamic range camera, to capture the entire light distribution in one measurement, rather than using the integrating sphere. The highest dynamic range in one of our measurements is 4400:1. Assuming an signal to noise ratio of 10:1, this would necessitate a high-end camera-sensor with a resolution of at least 16 bit. The lowest measured power is 34 nW.

A camera setup could also reduce the total size of the apparatus, which currently measures about 1000 mm. Instead of propagating the light over a long distance to capture the far-field pattern, the far-field pattern can also be captured by a camera sensor in the focal plane of a lens placed, as shown in Fig. 5.[11]

2.5 Effects of Compensation Error

To understand the effects of tilt and curvature errors on the diffraction pattern of otherwise flat structures, the simpler model of Fraunhofer diffraction is used to find the diffraction efficiencies for each order. As described in Ref. 11, the diffraction efficiency η_k describes the fraction of the total incident power diffracted into the k'th order of a periodic grating. If the field behind

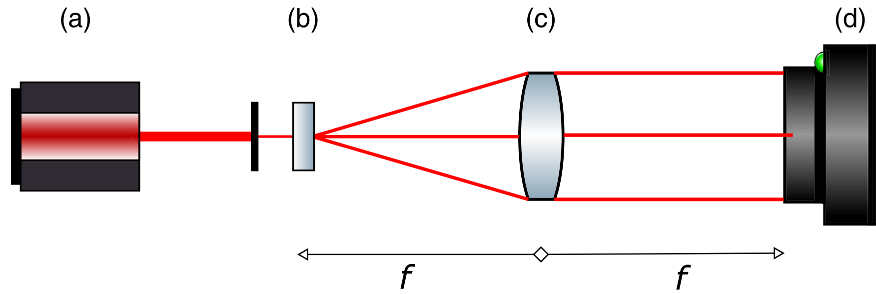

Fig. 5 Alternative measurement setup: the laser (a) emits coherent light, which passes through an aperture stop and the grating under test (b). The grating is placed in the focal plane of a lens (c). In the back focal plane, the far-field diffraction pattern is captured with a camera (d).

the grating can be expressed as a Fourier series with complex terms c_k, the diffraction efficiencies into each order are equal to the square of these terms

$$\eta_k = |c_k|^2. \tag{7}$$

For a structure containing only tilt errors, the field after the grating can be expressed as $U(x) = e^{-i \cdot a \frac{2\pi \cdot (n_0 - n_1)}{\lambda} \cdot x}$. Substituting $\phi_0 = a \cdot \frac{2\pi \cdot (n_0 - n_1)}{\lambda}$ the diffraction efficiencies simplify to

$$\eta_k = \left| \frac{1}{d} \int_{-\frac{d}{2}}^{\frac{d}{2}} e^{-i \cdot \phi_0 \cdot x} \cdot e^{\frac{-i 2\pi k x}{d}} \mathrm{d}x \right|^2 = \sin c^2 \left(k + \frac{\phi_0 \cdot d}{2\pi} \right). \tag{8}$$

Thus diffraction efficiency becomes maximal for $k = (-\phi_0 \cdot d/2\pi)$.[11] This means that an increase in tilt leads to an increase in light diffracted into the positive or negative higher orders. This behavior is illustrated in Fig. 6(a). This figure shows the first two positive and negative diffraction orders for different tilt values.

For the case of curvature errors, using the same substitution for ϕ_1, the diffraction efficiencies are

$$\eta_k = \left| \frac{1}{d} \int_{-\frac{d}{2}}^{\frac{d}{2}} e^{-i \cdot \phi_1 \cdot x^2} \cdot e^{\frac{-i 2\pi k x}{d}} \mathrm{d}x \right|^2. \tag{9}$$

This integral can be solved numerically. To demonstrate the influence of curvature, the diffraction efficiencies are calculated and shown for five different curvature values in Fig. 6(b).

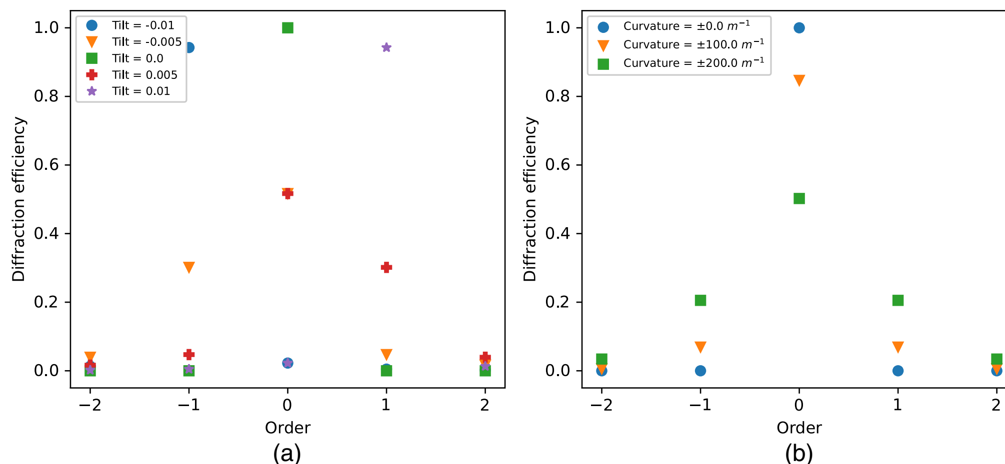

Fig. 6 Diffraction efficiencies for selected tilt and curvature values: the *y*-axis shows the diffraction efficiency, and the *x*-axis shows the diffraction order, for different tilt (a) and curvature (b) values. The diffraction efficiencies for positive and negative curvature are identical and thus they are shown as one point.

Table 1 Selected tilt and curvature values of test structures.

Tilt	0	1×10^{-3}	2×10^{-3}	4×10^{-3}	5×10^{-3}	6×10^{-3}
Curvature	0 m^{-1}	40 m^{-1}	80 m^{-1}	160 m^{-1}	200 m^{-1}	—

Two important observations can be made from this: (1) higher curvature values lead to a symmetrical increase in light diffracted into the higher orders and (2) positive and negative curvature errors cannot be distinguished from the intensity distribution. This means that the scatterometric setup cannot determine the sign of curvature errors. For our application, this problem can be solved by printing two different structures: one compensated assuming positive and one assuming negative curvature errors. The better one is then chosen. Additionally, it turned out that the sign of curvature errors is always negative with the used printer.

With this information, it is possible to determine the kind of error dominant on a flat structure: (1) if the diffraction orders are asymmetrical in x or y direction, there is a tilt in that direction. (2) If they are symmetrical in a direction, there is curvature. (3) If there are no tilt and curvature errors, all light is diffracted into the $0'$th order, as expected for a flat structure.

2.6 Fabrication of Test Structures

To evaluate the suggested technique for reconstruction three cases are considered.

- Predominant tilt errors: as demonstrated in Fig. 1, tilt errors are typically caused by a tilt error of the substrate holder relative to the optical axis. This has been observed to be the dominant error on the given printer. From experience, a typical tilt value of 3×10^{-3} (3 mrad) is estimated.
- Predominant curvature errors: some printers offer a built in tilt compensation. In this case, the curvature error caused by spherical aberrations will be the dominant error. For our printer, the typical curvature error is 100 m^{-1}.
- Mixture of tilt and curvature errors: in other cases, tilt and curvature errors may be of similar size and need to be compensated together. The proposed method does enable the reconstruction of both. To test this third case, four tilt values (0, 1×10^{-3}, 2×10^{-3}, and 5×10^{-3}) and four curvature values (0, 40, 80, and 200 m^{-1}) are chosen and all possible combinations of tilt and curvature errors are printed, resulting in a total of 16 different structures.

Table 1 shows the selected parameters for our test structures. All structures are printed using a TPP printer with an existing tilt and curvature compensation.

2.7 Confocal Analysis of Test Structures

To confirm the grating parameters of the test structures, seven periods are scanned with a confocal microscope. All profiles along the x-axis are extracted. Since there is no variation along the y-axis, the different profiles are averaged along the y-axis. A quadratic function is fit on each period, using orthogonal distance regression (ODR), and the seven sets of parameters are averaged. This is also illustrated in Fig. 7.

The variance of each parameter is estimated as the sum of two variances: the average variance of the fitted parameters as estimated by ODR routine and the variance between the seven values.

2.8 Compensation Based on Scatterometry Data

To use the extracted grating parameters for compensation, the structure height at each point of a stitching field is calculated based on Eq. (1). A height map of one stitching field is saved as a gray-scale image, called compensation image. Figure 8 shows a typical compensation image and the structure it represents.

This image, along with the corresponding dimensions, can be loaded into print projects, and will then be subtracted from each stitching field in the print. By applying this compensation technique, we print both a flat structure and a DOE. The image of this DOE is compared to the same DOE printed without a compensation. The flat structure is examined with confocal microscopy, as described in Sec. 2.7, to determine the residual tilt and curvature errors.

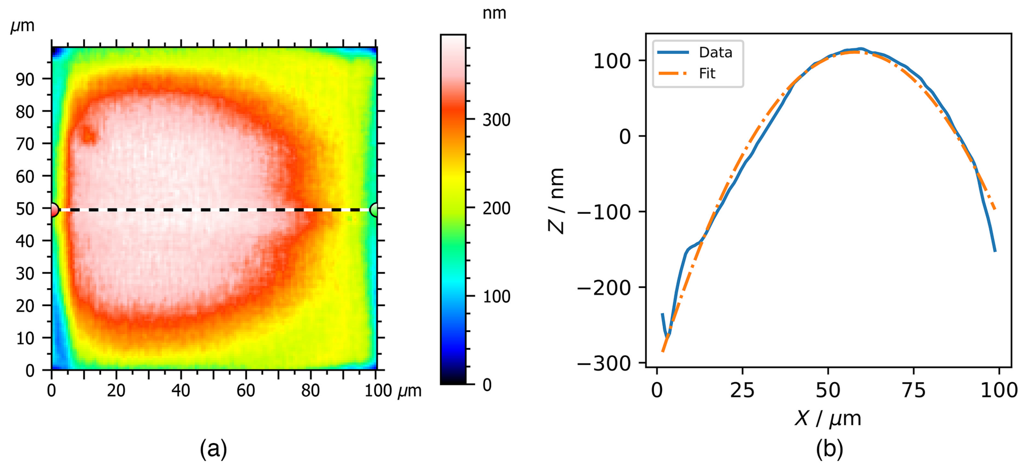

Fig. 7 Color coded height map of one measured stitching field without compensation (a) and extracted profile with quadratic fit (b). One period of the grating as measured with the confocal microscope. The profile along one direction is extracted and a second-degree polynomial is fitted to the data.

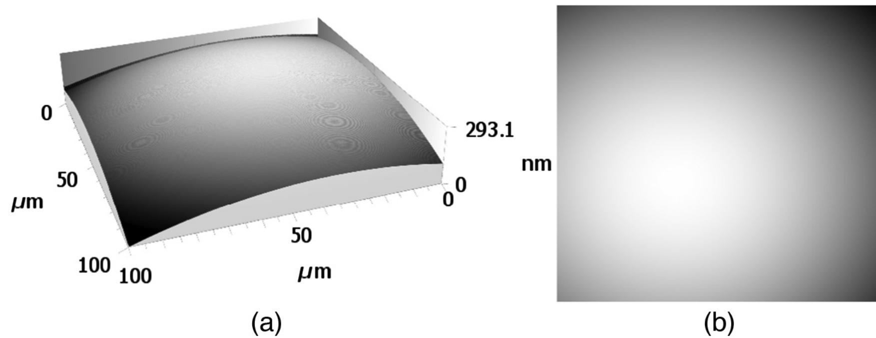

Fig. 8 Three-dimensional structure (a) and its corresponding compensation image (b). The image represents the structure's height through grayscale values and provides complete surface information when dimensions in the x, y, and z direction are known.

3 Results

3.1 Tilt Error Reconstruction

To evaluate the reconstruction of tilt parameters, the reconstructed parameters are compared to the values obtained from confocal measurements, as described in Sec. 2.7. Ideally, both would be identical. This behavior is shown on the blue line in Fig. 9(a). The x-axis shows the tilt error measured by a confocal microscope, and the y-axis shows the tilt error reconstructed from scatteromerty data. The measured data points are shown as orange dots, with error bars corresponding to the estimated 1σ uncertainties. For the reconstructed value, the uncertainties are estimated by the least-squares minimization function, and for the confocal measurement, they are estimated, as described in Sec. 2.7.

The plot shows a strong correlation between the two measurements. This can be quantified by the r^2 value (square of the empirical Pearson coefficient[12]). We obtain an r^2 of 0.9, confirming a strong correlation between confocal measurement and the reconstructed grating parameters for tilt errors. To assess the precision of the reconstructed tilt errors, the standard deviation of the parameter is estimated as the square root of the average sum of squares of the differences between the confocal measurements p_i and the corresponding reconstructed value q_i: $\sigma = \sqrt{\frac{1}{n-1}\sum_{i=1}^{n}(p_i - q_i)^2}$. The estimated uncertainty is 9×10^{-4} (0.9 mrad), which is about

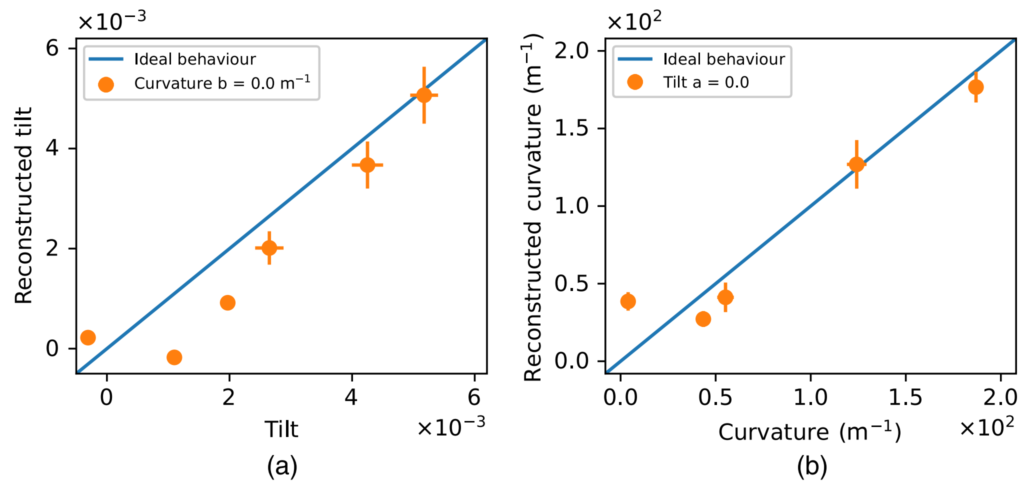

Fig. 9 Reconstructed tilt (a) and curvature (b) values for the test structures only containing either tilt or curvature errors. The error bars show 1σ uncertainties estimated by the minimization routine. The blue line shows the ideal behavior, where reconstructed tilt and actual tilt are identical.

three times smaller than the assumed typical tilt errors. This indicates that the proposed method is applicable for tilt error correction.

3.2 Curvature Error Reconstruction

Curvature reconstruction is evaluated in the same way as tilt error reconstruction. As discussed in Sec. 2.5, we restrict the investigation of curvature errors to the absolute values. The results are shown in Fig. 9(b). Again, a strong correlation can be demonstrated, which is confirmed by the high coefficient of correlation $r^2 = 0.92$. The estimated uncertainty is 21 m^{-1}, which is five times smaller than the assumed curvature of 100 m^{-1}, indicating high applicability for curvature errors as well.

3.3 Tilt and Curvature Reconstruction

In the most general case, tilt and curvature errors occur simultaneously. As in the previous cases, Fig. 10 shows the reconstructed tilt (a) and curvature (b) values on the y-axis and the confocal measurements on the x-axis. The blue line indicates the ideal behavior, and the measured data points are shown as dots. For the variation of tilt, the color of the dots indicates the different

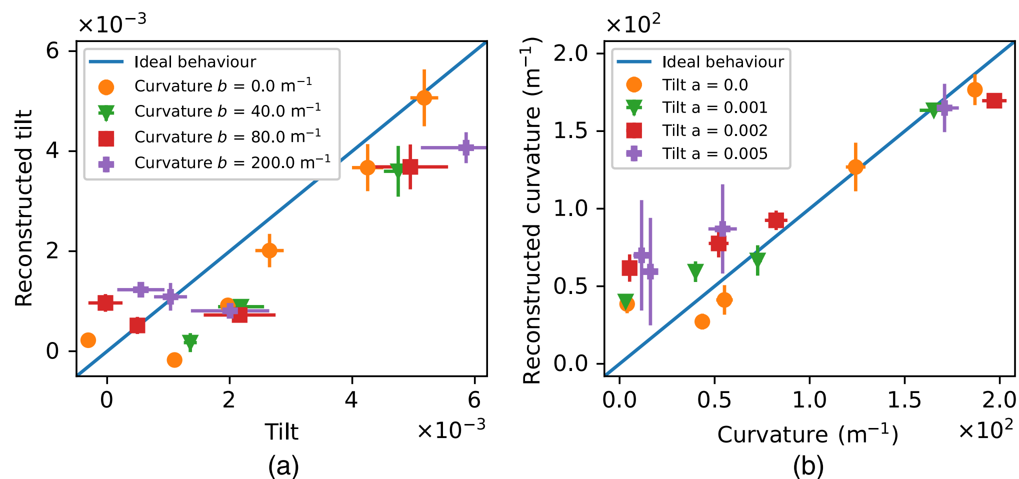

Fig. 10 Reconstructed tilt (a) and curvature (b) values for the test structures containing both tilt and curvature errors. The error bars show 1σ uncertainties estimated by the minimization routine. The blue line shows the ideal behavior, where reconstructed tilt errors and actual tilt errors are identical.

Table 2 Residual errors after the compensation and errors before compensation: The dominant *x*-tilt could be reduced by more than a factor of 4 with the new compensation method. The other fabrication errors remain in their low regime.

	X		*Y*	
	Tilt	Curvature	Tilt	Curvature
Uncompensated	$-9.4 \pm 1.5 \times 10^{-4}$	-59 ± 5 m^{-1}	$1.1 \pm 1.4 \times 10^{-4}$	-59.1 ± 1.3 m^{-1}
Compensated	$-2.2 \pm 1.9 \times 10^{-4}$	-58 ± 6 m^{-1}	$2.2 \pm 1.6 \times 10^{-4}$	-69 ± 2 m^{-1}

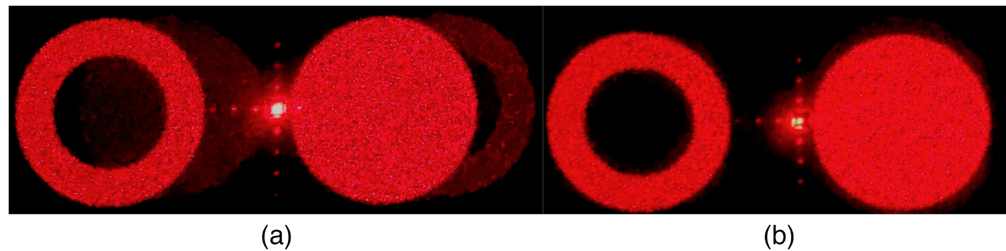

(a) (b)

Fig. 11 Comparison of diffraction pattern of an uncompensated DOE (a) and a DOE compensated with the Fourier scatterometry (FS) setup (b). Both images are taken with identical camera settings. In the compensated DOE, the conjugate noise and the DC noise are clearly reduced. The DC noise power is reduced by a factor of 12.

curvatures that occur at the same time, and for the variation of curvature, it indicates tilt. A correlation is again visible in both cases. For tilt errors, r^2 equals 0.82, and for curvature errors, r^2 equals 0.85. The uncertainties are estimated as described before. For tilt errors, the uncertainty is 1.1×10^{-3}, and for curvature errors, it is 40 m^{-1}. While the uncertainties are larger than in the two previous cases, a separate measurement of tilt and curvature errors is still possible.

3.4 Compensation

Table 2 shows the measurement results of the new printed structure using compensation parameters determined by Fourier scatterometry. The dominant tilt error (*x*-domain) is reduced by more than a factor of 4. Thus it is now in the same area as the *y*-direction tilt, both within the expected measurement uncertainties, as discussed in Sec. 3.3. The same applies to curvature compensation, which is already low in the uncompensated case.

To further demonstrate the effect of the compensation, the DOEs with and without compensation are evaluated. They are illuminated with a laser and the resulting far-field image is captured with a camera. Both images are taken with identical camera settings. The far-field image of the printed DOE represents the logo of Bonn-Rhein-Sieg University. Figure 11 shows the diffraction pattern of the DOE without compensation (a) and with compensation (b). The compensation leads to a significant reduction in noise: in the compensated DOE, the conjugate noise, visible as a darker mirrored version of the image in the uncompensated DOE, is no longer visible. Additionally, the direct component (DC) noise, which is the intensity of the 0′th order, is reduced from 109 to 8.88 μW, when illuminating the DOE with a 1 mW laser.

4 Conclusion

An FS setup for the compensation of tilt and curvature errors in TPP printers is introduced. The reconstructed grating parameters show a strong correlation to the grating parameters measured with a confocal microscope. The uncertainty of the reconstructed parameters is lower than the expected parameters for the printer. A tilt and curvature compensation determined with this setup significantly reduces DC and conjugate noise in the diffraction image of a printed DOE. This verifies a successful reduction of the errors that are inherent to the used TPP printer.

Thus, with this setup, we could demonstrate a low cost compensation, capable of substituting measurements with an expensive confocal microscope.

Since the discussed setup is kept very simple so far, further improvements in precision can be expected from future work. We can expect better calibration quality compared to using confocal microscopy since FS is not limited by the diffraction limit. Actual starting points for improvement are: the use of an RCWA forward model, measuring the laser intensity distribution, measuring at different polarizations and measuring at multiple wavelengths. Additionally, an improved automated setup, using an electronic linear translation stage or a high dynamic range camera to capture the intensity distribution, is expected to yield improved results.

Code, Data, and Materials Availability

The used code and data are uploaded to Code Ocean.[13]

Acknowledgments

This work was partly supported by the Federal Office of Information Security (BSI, Project BIOLAB), the Institute of Safety and Security Research (ISF) and the Department of Engineering and Communication (DEC) of Hochschule Bonn-Rhein-Sieg.

References

1. S. O'Halloran et al., "Two-photon polymerization: fundamentals, materials, and chemical modification strategies," *Adv. Sci.* **10**(7), 2204072 (2023).
2. H.-B. Sun and S. Kawata, *Two-Photon Photopolymerization and 3D Lithographic Microfabrication*, pp. 169–273, Springer Berlin Heidelberg, Berlin, Heidelberg (2004).
3. R. K. Leach et al., "*Guide to the measurement of smooth surface topography using coherence scanning interferometry*," Measurement Good Practice Guide (2008).
4. M. Conroy and J. Armstrong, "A comparison of surface metrology techniques," *J. Phys. Conf. Ser.* **13**(1), 458 (2005).
5. V. Paz et al., "Development of functional sub-100 nm structures with 3D two-photon polymerization technique and optical methods for characterization," *J. Laser Appl.* **24**, 042004 (2012).
6. N. Kumar et al., "Reconstruction of sub-wavelength features and nano-positioning of gratings using coherent Fourier scatterometry," *Opt. Express* **22**, 24678–24688 (2014).
7. C. Raymond, "Overview of scatterometry applications in high volume silicon manufacturing," *AIP Conf. Proc.* **788**(1), 394–402 (2005).
8. F. Shen and A. Wang, "Fast-Fourier-transform based numerical integration method for the Rayleigh–Sommerfeld diffraction formula," *Appl. Opt.* **45**, 1102–1110 (2006).
9. L. S. Brea, "Diffractio, Python module for diffraction and interference optics," (2019).
10. P. Virtanen et al., "SciPy 1.0: fundamental algorithms for scientific computing in Python," *Nat. Methods* **17**, 261–272 (2020).
11. J. W. Goodman, *Introduction to Fourier Optics*, 3rd ed., W.H. Freeman, New York (2005).
12. T. Becker et al., *Stochastische Risikomodellierung Und Statistische Methoden*, Statistik Und Ihre Anwendungen, 1st ed., Springer, Berlin, Germany (2016).
13. E. Ellingen et al., "Fourier scatterometry for compensation of tilt and curvature deviations of two photon polymerization 3d printers [Source Code]," https://doi.org/10.24433/CO.3055138.v1 (2023).

Elias Ellingen is a master's student at Bonn-Rhein-Sieg University (Sankt Augustin). He completed his bachelor's degree in 2022, working on spectroscopy systems at the German Aerospace Agency (DLR). Since then, he has been working at Hochschule Bonn Rhein Sieg in the field of diffractive micro optics and TPP printing.

Markus Rohde received his master's degree in engineering (MEng) in 2020, after completing his studies at Bonn-Rhein-Sieg University (Sankt Augustin). He did his research in the field of radiation measurement on aircraft and space at DLR (Cologne). Since 2020, he has been a doctoral student at H-BRS and University of Siegen and is working in the field of photonic systems.

Bastian Stahl completed his master's degree in electrical engineering in 2022 at Bonn-Rhein-Sieg University (Sankt Augustin). Since 2022, he has been a doctorate student there. His work focuses on optical measurement technology and system integration.

Robert Lange received his PhD in engineering from the University of Siegen in 2000, after completing his doctorate at CSEM (Zurich). From 2000 to 2003, he was a project manager at GretagMacbeth (Regensdorf) in the field of color measurement. From 2003 to 2018, he was head of development at pmdtechnologies (Siegen) with focus on 3D ToF imagers and systems. Since 2018, he has been working as a professor for electronics and photonics at Bonn-Rhein-Sieg University (Sankt Augustin).